Radiotherapy diagnostic biomarkers in radioresistant human H460 lung cancer stem-like cells

Hong Shik Yun, Jeong-Hwa Baek, Ji-Hye Yim, Hong-Duck Um, Jong Kuk Park, Jie-Young Song, In-Chul Park, Jae-Sung Kim, Su-Jae Lee, Chang-Woo Lee & Sang-Gu Hwang

Taylor & Francis
Taylor & Francis Group

RESEARCH PAPER

OPEN ACCESS

Radiotherapy diagnostic biomarkers in radioresistant human H460 lung cancer stem-like cells

Hong Shik Yun[a,b], Jeong-Hwa Baek[a,c], Ji-Hye Yim[a], Hong-Duck Um[a], Jong Kuk Park[a], Jie-Young Song[a], In-Chul Park[a], Jae-Sung Kim[a], Su-Jae Lee[a], Chang-Woo Lee[c], and Sang-Gu Hwang[a]

[a]Division of Radiation Cancer Biology, Korea Institute of Radiological and Medical Sciences, Seoul, South Korea; [b]Department of Life Science, College of Natural Sciences, Hanyang University, Seoul, South Korea; [c]Department of Molecular Cell Biology, Samsung Biomedical Research Institute, Sungkyunkwan University School of Medicine, Suwon, South Korea

ABSTRACT

Tumor cell radioresistance is a major contributor to radiotherapy failure, highlighting the importance of identifying predictive biomarkers for radioresistance. In this work, we established a radioresistant H460 (RR-H460) cell line from parental radiosensitive H460 lung cancer cells by exposure to fractionated radiation. The radiation-resistant, anti-apoptotic phenotype of RR-H460 cell lines was confirmed by their enhanced clonogenic survival and increased expression of the radioresistance genes Hsp90 and Her-3. RR-H460 cells displayed characteristics of cancer stem-like cells (CSCs), including induction of the surface marker CD44 and stem cell markers Nanog, Oct4, and Sox2. RR-H460 cells also exhibited sphere formation and malignant behavior, further supporting a CSC phenotype. Using proteomic analyses, we identified 8 proteins that were up-regulated in RR-H460 CSC lines and therefore potentially involved in radioresistance and CSC-related biological processes. Notably, 4 of these—PAI-2, NOMO2, KLC4, and PLOD3—have not been previously linked to radioresistance. Depletion of these individual genes sensitized RR-H460 cells to radiotoxicity and additively enhancing radiation-induced apoptosis. Our findings suggest the possibility of integrating molecular targeted therapy with radiotherapy as a strategy for resolving the radioresistance of lung tumors.

Abbreviations: CSCs, cancer stem-like cells; NSCLC, non-small cell lung cancer; PARP, poly ADP-ribose polymerase; RR-H460, radioresistant H460; siRNA, small interfering RNA.

Introduction

Lung cancer is one of the most common and serious types of cancer in the world, and the most prominent lung cancer is non-small cell lung cancer (NSCLC), accounting for about 85% to 90% of all lung cancer diagnoses.[1] Although treatment of lung cancer depends on the type and stage of the cancer, the main types of treatment are surgery, radiotherapy, and chemotherapy. Biological or targeted therapies can also help control the growth of advanced lung cancer for a time.[2] Radiotherapy in particular, used in combination with chemotherapy and/or surgery, which exerts synergistic effects, plays an important role in treating NSCLC.[3] Despite of treatment, 5-year survival rates for NSCLC patients are poor.

A major cause of the high mortality rate in NSCLC patients is the development of radioresistance, and overcoming radioresistance in NSCLC is an important current challenge. In this context, identification of novel diagnostic biomarkers for radioresistance has been a goal of the radiation cancer research field.

Studies to date have shown that tumor radioresistance is associated with specific molecules, shedding some light on the mechanisms of cellular radioresistance. For example, p53 and members of the Bcl-2 family, as apoptosis modulators, regulate the radioresistance phenotype of lung and pancreatic cancers.[4,5] Proliferation-regulating proteins of the Ras/Raf family are constitutively activated and mediate radioresistance of laryngeal cancer.[6,7] Phosphoinositide 3-kinase/Akt, a major downstream target of epidermal growth factor receptor signaling, plays an important role in radioresistance mechanisms in head-and-neck cancer.[8] Hepatoma-derived growth factor-related protein 3, whose biological functions are largely unclear, was initially reported as a radioresistance-regulating protein in NSCLC cells.[9,10] Up-regulation of the proangiogenic factor ephrin-A1 has also been reported to regulate murine tumor radioresistance.[11] Although accumulating evidence suggests the potential of radioresistance-associated factors as biomarkers and/or novel therapeutic targets, such factors in NSCLC cells and their molecular mechanisms remain largely unknown.

High-throughput analyses can predict targets that are associated with tumor radioresistance. For example, Guo et al. compared two lung cancer cell lines, H446 and A549, using oligonucleotide microarrays to identify radioresistance regulatory genes.[12] Lee et al. performed microarray analyses using radioresistant H460 (RR-H460) cells established from parental

H460 cells and found altered expression of 1,463 genes.[13] A recently emerging technique for the large-scale experimental analysis of proteins is proteomics. By applying proteomic analyses in radioresistant HEp-2 laryngeal cancer cells, we previously reported 16 radioresistance-related proteins.[14] Although some cancer cells develop radioresistance as a result of the function of specific target proteins, the protein profiles associated with radioresistance in NSCLC cells and underlying molecular mechanisms of resistance development are poorly understood.

In this study, we established RR-H460 cells through exposure of parental H460 NSCLC cells to fractionated γ-ray irradiation and found that these cells displayed a cancer stem-like cell (CSC) phenotype. Using proteomic analyses, we identified 4 candidate radioresistance regulatory proteins—plasminogen activator inhibitor 2 (PAI-2), nodal modulator 2 (NOMO2), kinesin light chain 4 (KLC4) and procollagen-lysine 2-oxoglutarate 5-dioxygenase 3 (PLOD3)—whose expression levels were increased in RR-H460 CSCs. Therefore, our findings suggest possible alternative treatment strategies that could be considered for NSCLC patients who are unresponsive to radiotherapy.

Results

Establishment of human RR-H460 NSCLC cell lines

After cumulative treatment of H460 cells with 2-Gy radiation twice a week for 20 wk, radiation sensitivity was determined using clonogenic survival assays. Colony formation markedly increased in the RR-H460 cell population (termed RR-Full) and isolated RR-H460 subclones (RR-#2 and RR-#5) compared with H460 cells after single exposure to radiation ranging from 0 to 6 Gy (Fig. 1A). RR-H460 cell lines (RR-Full, RR-#2, and RR-#5) showed a distinct radioresistance phenotype, as determined by survival fraction analysis (Fig. 1B). They were also more proliferative than parental H460 cells without treatment (Fig. 1C) and following treatment with 6-Gy radiation (data not shown). Consistent with these results, exposure to 10-Gy radiation induced approximately 47% cell death in H460 cells compared with the corresponding values of 27%, 16%, and 18% in RR-Full, RR-#2, and RR-#5 cells, respectively (Fig. 1D). Levels of cleaved poly ADP-ribose polymerase (PARP) (Fig. 1E, top) and degree of nuclear blebbing (Fig. 1E, bottom) were highly induced in radiation-treated H460 cells, whereas these 2 apoptotic indicators were dramatically suppressed in radiation-
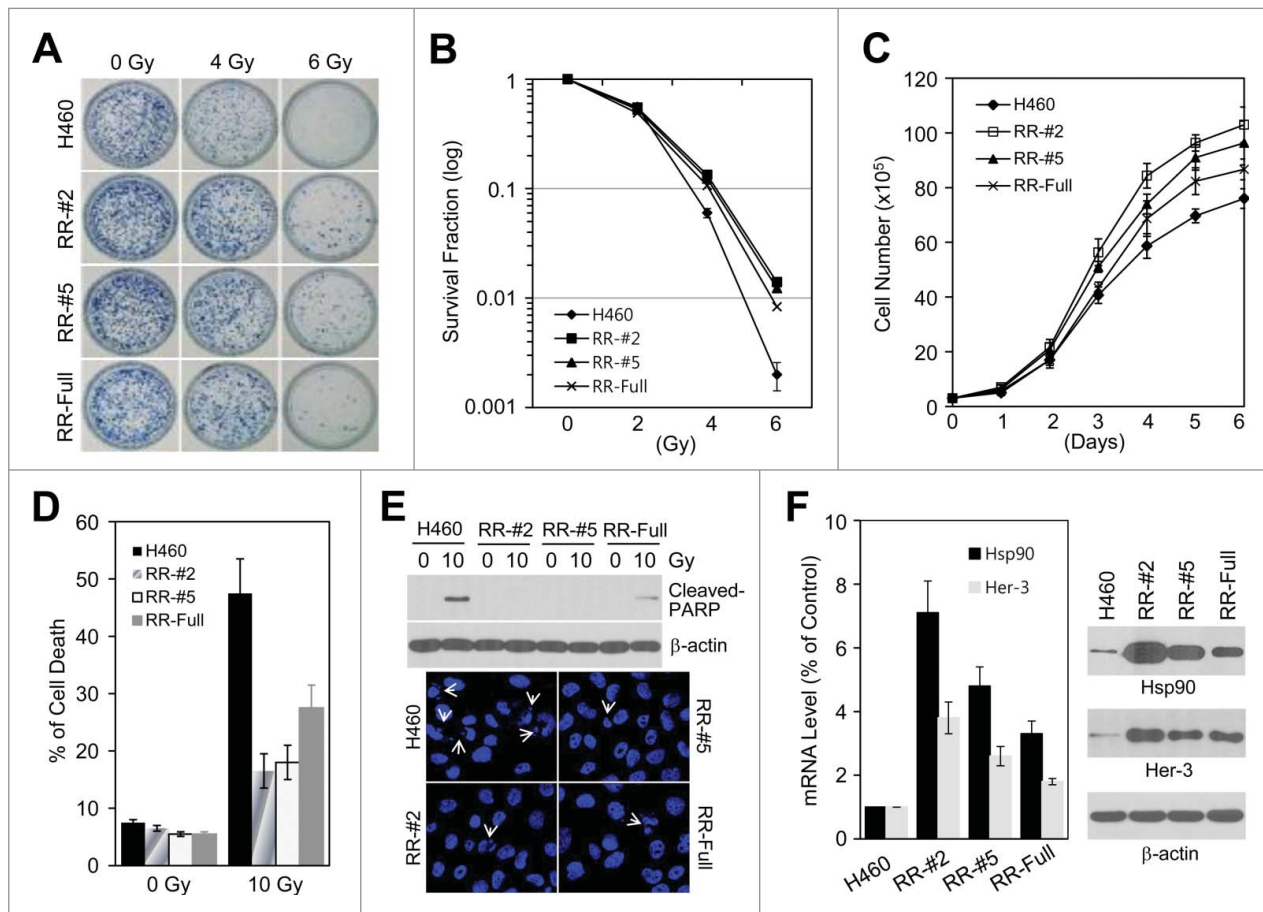
Figure 1. Establishment of RR-H460 cell lines. H460 cells were treated with 2-Gy radiation twice a week for 20 wk. (A and B) H460, RR-Full, RR-#2, and RR-#5 cell lines were left untreated or were treated with 2–6-Gy radiation for 14 d. Colony formation was visualized by trypan blue staining (*A*) and cell survival data were plotted as logarithm of the survival fraction (*B*). (C) Cells were seeded at a density of 3×10^5 cells per 60-mm plate. On the indicated days, the total number of cells was quantified by counting the surviving cells using trypan blue solution. (D and E) H460, RR-Full, RR-#2, and RR-#5 cell lines were left untreated or were treated with 10-Gy radiation and then cultured for 48 h. Cell viability was determined by FACS analysis, and data are presented as the percentage of PtdIns-positive cells (*D*). Levels of cleaved PARP protein were determined by Western blotting using β-actin as the loading control (*E, top*), and the degree of nuclear blebbing was determined by DAPI (4′,6-diamidino-2-phenylindole) staining (*E, bottom*). (F) *Left*: Transcript levels of Hsp90 and Her-3, determined by qRT-PCR. *Right*: Protein levels of Hsp90 and Her-3, determined by Western blotting. The data represent typical results or mean values with standard deviations (n = 3).

treated RR-H460 cell lines. To further confirm the radioresistance phenotype, we examined transcription levels of genes encoding the known tumor radioresistance factors Hsp90 and Her-3.[15,16] As shown in Fig. 1F, quantitative reverse transcription-polymerase chain reaction (qRT-PCR, left) and Western blot analyses (right) showed that mRNA and protein levels of both genes were markedly increased in RR-H460 cell lines compared with H460 cells. Taken together, our results clearly demonstrate the radioresistance of the RR-H460 cell lines established here.

Characterization of CSC phenotype in RR-H460 cell lines

To define the CSC characteristics of RR-H460 cell lines, we analyzed the expression of the CSC surface markers, CD44 and CD133, by flow cytometry. Very small percentages (0.1–0.3%) of cells were CD133 positive in all tested cell lines, whereas 88%, 96%, and 95% of RR-Full, RR-#2, and RR-#5 cells, respectively, were CD44 positive compared to 82% of H460 cells (Fig. 2A). We next analyzed the expression profiles of CSC-related protein markers by Western blotting. RR-H460 cell lines highly expressed CD44 protein and activated Notch1 protein compared with H460 cells

(Fig. 2B). In addition, the pluripotency-associated transcription factors Nanog, Oct4 and Sox2, as well as the co-transcriptional regulator β-catenin, were markedly upregulated in RR-H460 cell lines compared with H460 cells (Fig. 2B), indicating the "stemness" status of RR-H460 cells. Moreover, the number of spheres on day 5 in nonadherent cultures was significantly increased in CD44-highly expressing RR-H460 cell lines compared to H460 cells (Fig. 2C, left). The average number of spheres per field was determined to be 29, 46, and 43 in RR-Full, RR-#2, and RR-#5 cells, respectively, compared to only 6 in H460 cells (Fig. 2C, right). Under adhesion-culture conditions, this spherical morphology showed a rapid, time-dependent shift toward a spreading tumor cell phenotype (Fig. 2D). Taken together, our results suggest that RR-H460 cell lines maintain a lung CSC phenotype through activation of traditional CSC-related signaling pathways.

RR-H460 CSCs have a more aggressive malignant phenotype than parental H460 cells

Because CSCs are associated with a dynamic, malignant cancer cell phenotype, we tested the properties of RR-H460 CSC lines. RR-Full, RR-#2, and RR-#5 cell lines exhibited
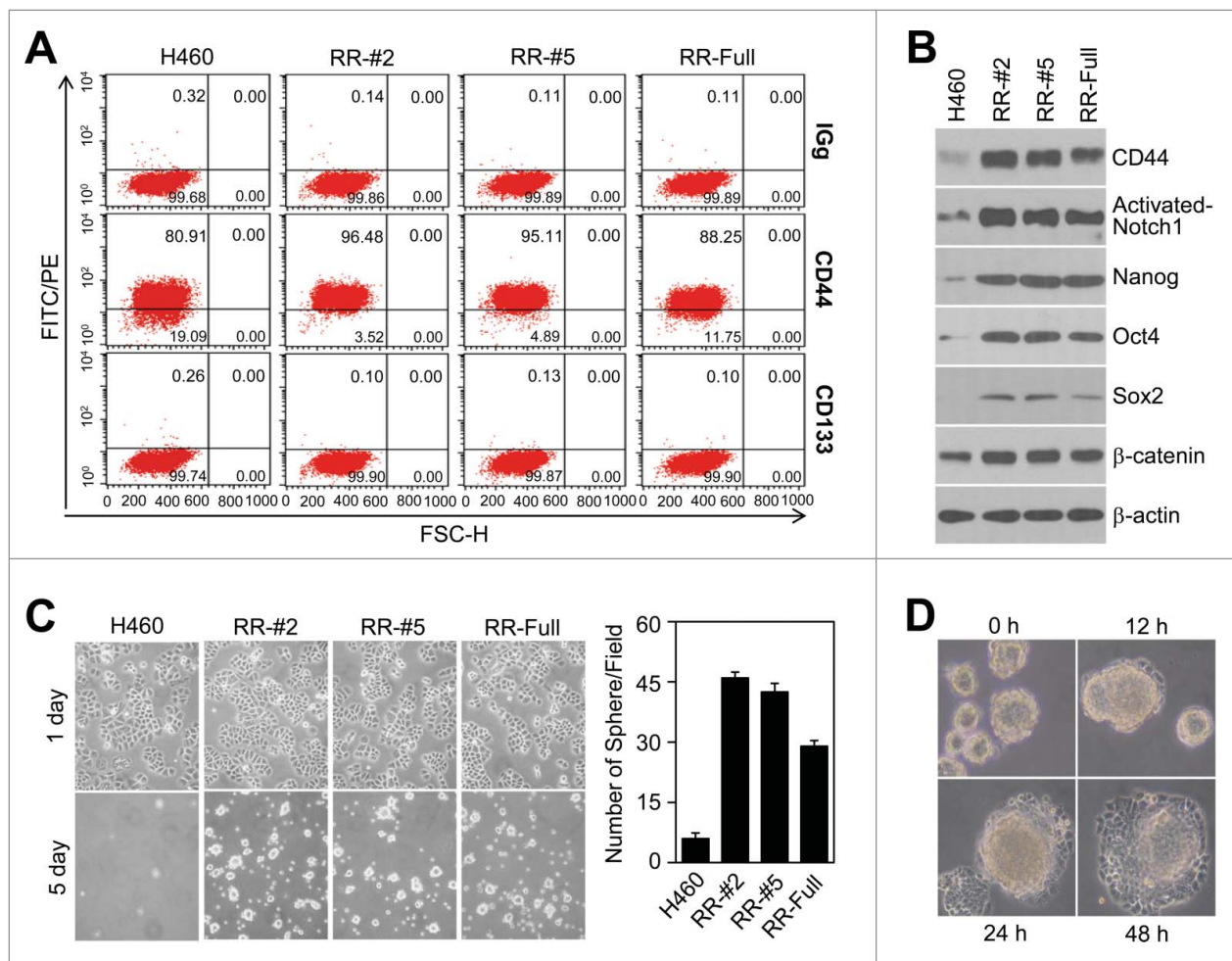
Figure 2. Characterization of the CSC phenotype in RR-H460 cell lines. (A) CD44 and CD133 expression profiles were characterized by FACS analysis. Cells in suspension were labeled with FITC-conjugated anti-CD44 and PE-conjugated anti-CD133 antibodies. Isotype controls were used to establish the appropriate gating. (B) Levels of CSC-related proteins were determined by Western blotting using β-actin as the loading control. (C) *Left*: Morphology of tumor spheres formed from adherent populations, observed by light microscopy. *Right*: Quantification of spheres. (D) Spheres formed by RR-#2 cells were exposed to serum and then morphology was observed by light microscopy at each time point. The data represent typical results or mean values with standard deviations (n = 3).

significantly enhanced invasion (Fig. 3A, left) and migration (Fig. 3B, left) behavior compared with H460 cells, as determined by Matrigel transwell invasion assay. Specifically, compared with parental H460 cells, the invasion rate was increased approximately 1.7-, 2.6-, and 2.2-fold in RR-Full, RR-#2, and RR-#5 cells, respectively (Fig. 3A, right); the corresponding increases in migration rate were approximately 1.8-, 2.9-, and 2.7-fold (Fig. 3B, right). RR-H460 cell lines also exhibited a marked, time-dependent increase in mobility compared with H460 cells, as determined by wound-healing assays (Fig. 3C). In addition, colony-forming assays revealed enhanced cell growth effects in RR-H460 cell lines compared with H460 cells (Fig. 3D, left), showing that proliferation rate was increased approximately 1.7-, 2.5-, and 2.2-fold in RR-Full, RR-#2, and RR-#5 cells, respectively (Fig. 3D, right). These data suggest that RR-H460 cell lines exhibit CSC-like aggressive cellular behaviors and thus strongly manifest a malignant cancer phenotype.

Suppression of cellular senescence in RR-H460 CSCs

To examine whether cellular senescence is inhibited in RR-H460 cell lines, we treated cells with doses of radiation ranging from 0 to 6 Gy. As shown in Fig. 4A, radiation induced a dose-dependent change in H460 cell shape toward a large, flattened morphology and increased senescence-associated β-galactosidase (SA-β-gal) staining. These effects were blunted in RR-Full and RR-#2 cell lines. In particular, the percentage of SA-β-gal–positive cells was approximately 32% and 23% in 6-Gy–treated RR-Full and RR-#2 cells, respectively, compared to 52% in 6-Gy–treated H460 cells. Senescence inhibition in RR-Full and RR-#2 cell lines was confirmed by assessment of specific senescent-associated biochemical markers. Radiation treatment induced much higher expression and activation levels of the canonical senescence-associated protein p53 in H460 cells compared to RR-H460 cell lines (Fig. 4B). Both p21 and p16 protein levels were also very strongly elevated by radiation treatment in H460 cells, but were dramatically reduced in RR-H460 cell lines under the same conditions (Fig. 4B). Consistent with upregulation of senescence markers, radiation treatment significantly induced G_2/M cell cycle arrest in H460 cells. At 12 and 24 h, the percentages of cells in G_2/M were approximately 56% and 45%, respectively, in H460 cells (Fig. 4C, left), but were reduced to 37% and 27%, respectively, under the same conditions in RR-#2 cells (Fig. 4C, right). These results suggest that cell proliferation
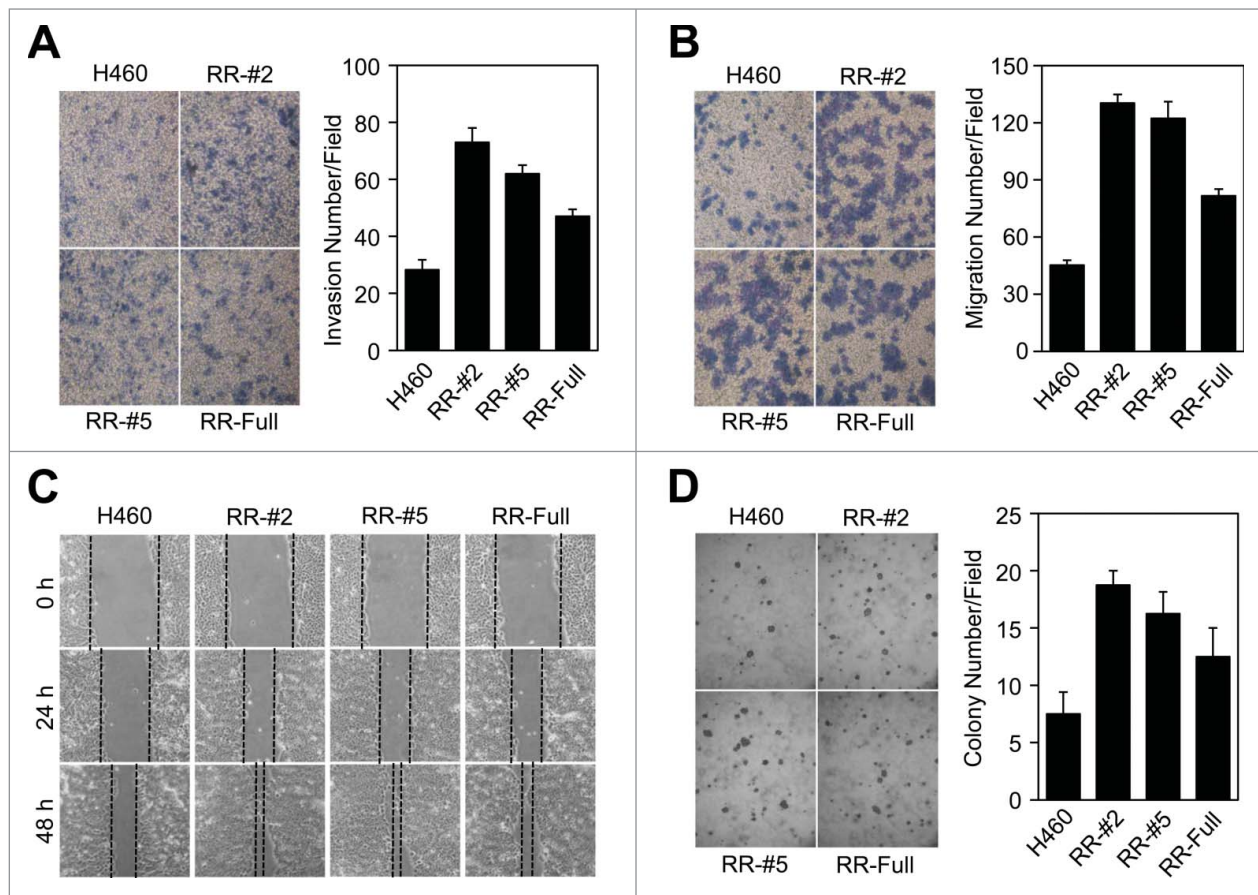
Figure 3. Characterization of the malignant phenotype in RR-H460 cell lines. (A and B) H460, RR-Full, RR-#2, and RR-#5 cell lines were seeded in Matrigel-coated (*A*) or uncoated (*B*) Transwells and allowed to invade for 18 h. Invading or migrating cells were stained with Coomassie blue, visualized by light microscopy, and counted. *Left*: Representative images of fields randomly selected in a blinded manner. *Right*: Quantification of cells. (C) Confluent cells were scratched with a micropipette tip, and images were obtained 24 and 48 h after creating the scratch. (D) H460, RR-Full, RR-#2, and RR-#5 cell lines were cultured for 15 d. *Left*: Representative images of fields randomly selected in a blinded manner. *Right*: Quantification of cells. The data represent typical results or mean values with standard deviations (n = 4).
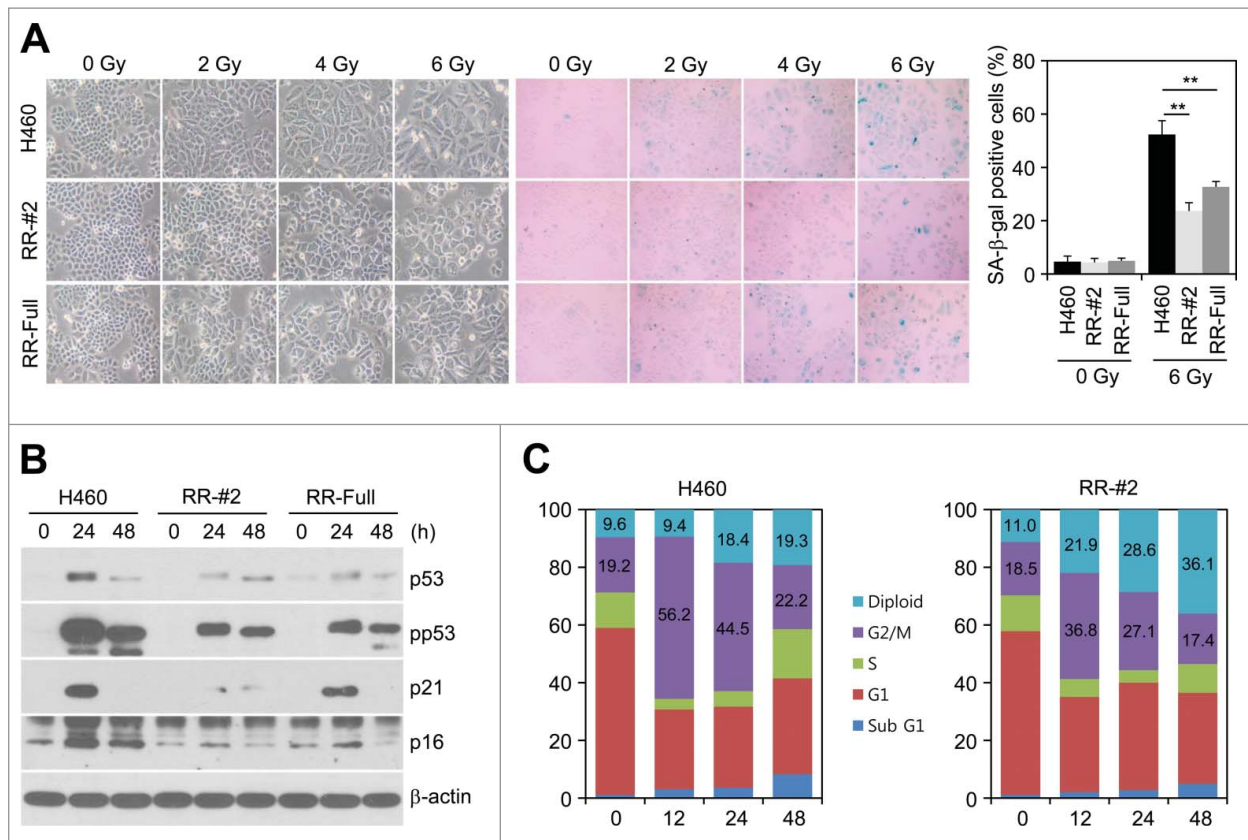
Figure 4. Inhibition of cellular senescence in RR-H460 cell lines. (A) H460, RR-Full, and RR-#2 cell lines were treated with radiation ranging from 0 to 6 Gy and then cultured for 48 h. *Left*: Cell morphology observed by light microscopy. *Middle and right*: Cellular senescence evaluated by SA-β-gal staining. Photomicrographs depict SA-β-gal–positive cells (blue; middle). Percentages of SA-β-gal–positive cells were determined by manually counting a total of 200 cells (right); data are expressed as means $\pm$ SD (**p < 0.005 compared with 6-Gy-radiation–treated H460 cells). (B) H460, RR-Full, and RR-#2 cells were treated with 6-Gy radiation and then incubated for the indicated periods. Expression and phosphorylation levels of p53, p21, and p16 proteins were detected by Western blotting using β-actin as the loading control. (C) H460 and RR-#2 cells were treated with 6-Gy radiation and then incubated for the indicated periods. Cellular DNA content was determined by FACS analysis, gated for Hoechst 33258 fluorescence.

is enhanced in RR-H460 cells by virtue of diminished radiation-induced G_2/M cell cycle arrest.

Proteomic analyses of H460 cells and RR-H460 CSC lines

To identify proteins that are differentially expressed between RR-H460 cell lines and H460 cells, we analyzed the expression profiles of H460, RR-Full, and RR-#2 cells using 2-dimensional (2D) polyacrylamide gel electrophoresis (PAGE) analysis. An analysis of silver-stained gels after SDS-PAGE using ImageMaster 2D platinum software revealed that 8 protein spots showed more than a 2-fold change in expression (Fig. 5A), changes that were significant (Table 1). Magnified views of gel images for H460, RR-Full, and RR-#2 cells are shown in Fig. 5B. Each protein was successfully identified by MALDI-TOF (matrix-assisted laser desorption/ionization–time of flight) mass spectrometry analysis, which provided excellent peptide coverage and yielded a significant MASCOT score (Table 1 and Supplementary Fig. 1). Four of these differentially expressed proteins—fatty acid synthase (FASN), vimentin (VIM), 78 kDa glucose-regulated protein (GRP78) and ubiquinol-cytochrome *C* reductase complex core protein 1 (UQCRC1)—were previously identified as a radioresistance- or radiation response-related proteins.[17-20] FASN, VIM, GRP78, and UQCRC1 expression were increased by approximately 2.6-, 4.4-, 8.1-, and

2.4-fold, respectively, in RR-H460 cell lines compared with H460 cells (Table 2). These data strongly support the relevance of our 2D gel data and the radioresistant phenotype of RR-H460 cell lines. In addition, PAI-2, NOMO2, KLC4 and PLOD3, which were not previously linked with radioresistance, were also increased by approximately 2.6-, 6.7-, 6.0-, and 3.1-fold, respectively, in RR-H460 cell lines compared with H460 cells (Table 2). Up-regulated expression levels of these 4 proteins in RR-#2 cells were further confirmed by Western blot analysis (Fig. 5C, left). To characterize the roles of 4 proteins in acquired and intrinsic radioresistance, we compared protein levels between radiosensitive H460 and radioresistant A549 and H1299 cell lines. We found that PAI-2 and KLC4 proteins were overexpressed in A549 and H1299 cells compared to H460 cells, indicating the association of both acquired and intrinsic radioresistance (Fig. 5C, right). However, levels of NOMO2 and PLOD3 proteins were paralleled in cells tested, indicating H460 cell type specification for acquired radioresistnace phenotype (Fig. 5C, right).

Identification of novel radioresistance biomarkers in RR-H460 CSC lines

Because the functions of PAI-2, NOMO2, KLC4, and PLOD3 proteins in relation to tumor radioresistance were unknown,
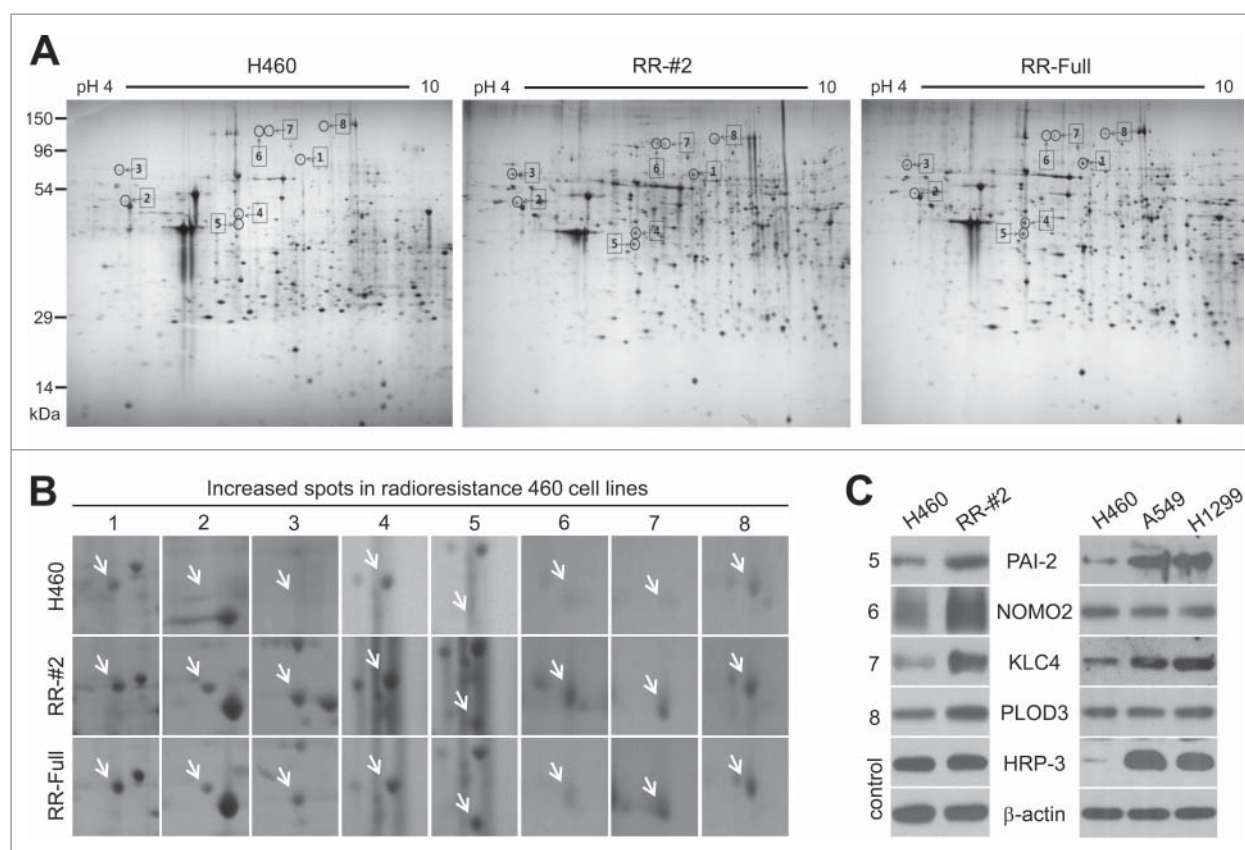
Figure 5. 2D gel analysis of proteins differentially expressed between H460 and RR-H460 cell lines. (A) H460, RR-Full, and RR-#2 cell lines were cultured for 48 h and cell lysates were collected from each cell line. Proteins (150 μg) were separated on an immobilized pH 4–10 gradient strip followed by SDS-PAGE on a 12% polyacrylamide gel. Proteins were visualized by silver staining and profiled using PdQuest software. Differentially expressed protein spots are marked by black arrows, with numbers on each panel. (B) Magnified views of 8 identified spots indicated in A. (C) *Left*: Increased levels of 4 novel radioresistance regulatory proteins (spots 5–8) were confirmed by Western blotting. HRP-3 and β-actin were used as negative control and loading control, respectively. *Right*: Comparison of spots 5–8 levels in 3 NSCLC cell lines. Data are presented as results of a typical experiment from 3 independent experiments.

we investigated their potential roles as radioresistance regulatory proteins. To this end, we knocked down each protein individually in RR-#2 CSCs using small inhibitory RNAs (siR-NAs) targeting the corresponding mRNAs. Transfection of siRNA targeting PAI-2 (siPAI-2), NOMO2 (siNOMO2), KLC4 (siKLC4), or PLOD3 (siPLOD3) in RR-#2 cells effectively knocked down the targeted protein (Fig. 6C). Although depletion of each individual upregulated protein in RR-#2

Table 1. List of differentially expressed protein between H460 and RR-H460 cells.

No.	Name	Fold change[a]	SD	Swiss-Prot Assession no.	Mw (kDa)	p/	Coverage[a]	MASCOT Score[c]	No. of matched peptide	Function
1	Fatty acid synthase (FASN)	(+)2.6	±0.71	P49327	275850	5.99	12	101	26	Fatty acid synthase activity
2	Vimentin (VIM)	(+)4.4	±0.27	P08670	53676	5.06	59	237	31	Structural constituent of cytoskeleton
3	78 kDa Glucose-regulated protein (GRP78)	(+)8.1	±0.26	P11021	72402	5.07	40	235	29	Protein binding
4	Ubiquinol cytochrome creductase core protein I (UQCRC1)	(+)2.4	±1.25	P31930	53297	5.94	53	203	26	Ubiquinol-cytochrome-c reductase activity
5	Plasminogen activator inhibitor 2 (PAI2)	(+)2.6	±0.33	P05120	46851	5.46	38	124	20	Serine-type endopeptidase inhibitor activity
6	Nodal modulator 2 (NOMO2)	(+)6.7	±0.78	Q5JPE7	135077	5.51	30	146	25	Carbohydrate binding
7	Kinesin light chain 4 (KLC4)	(+)6	±1.32	Q9NSK0	70965	5.95	20	74	11	Microtubule motor activity
8	Procollagen-lysine,2-oxoglutarate 5-dioxygenase 3 (PLOD3)	(+)3.1	±1.13	O60568	85302	5.69	43	292	35	L-ascorbic acid binding

In *t*-test, all changes were significant ($p < 0.05$).

[a] Fold change indicates mean value of spot volume ratio between RR-H460 cells and parental H460 cells in 4 independent experiments. (+) indicates increased protein expression in RR-H460 cells. SD indicates standard deviation of fold change in 4 independent experiments.

[b] Coverage means the ratio of the portion of protein sequence covered by matched peptides to the full length of the protein sequence.

[c] Mascot Score describes the significance of the search result from the search engine Mascot based on ions score, which is $-10^{*}Log(P)$, where P is the probability that the observed match is a random event.

Table 2. List of identified proteins and their radioresistance.

Protein	Expression[a]	Radioresistance	Reference
Fatty acid synthase (FASN)	↑ 2.6	Radioresistance	[17]
Vimentin (VIM)	↑ 4.4	Radioresistance	[18]
78 kDa Glucose-regulated protein (GRP78))	↑ 8.1	Radioresistance	[19]
Ubiquinol cytochrome c reductase core protein I (UQCRC1)	↑ 2.4	Radiation response	[20]
Plasminogen activator inhibitor 2 (PAI2)	↑ 2.6	Radioresistance	This study
Nodal modulator 2 (NOMO2)	↑ 6.7	Radioresistance	This study
Kinesin light chain 4 (KLC4)	↑ 6.0	Radioresistance	This study
Procollagen-lysine,2-oxoglutarate 5-dioxygenase 3 (PLOD3)	↑ 3.1	Radioresistance	This study

[a] Expression indicates increase of the protein expression in RR-H460 cells compared with H460 cells.

cells induced a different degree of cell death, a clear apoptotic effect was detected in the absence of any other stimulation, as evidenced by a change in cell morphology (Fig. 6A, top). siRNA-mediated knockdown of these proteins in RR-#2 cells also additively promoted cell death in combination with exposure to 10-Gy radiation (Fig. 6A, bottom). As a negative control, siRNA-mediated knockdown of HRP-3, alone or in combination with radiation, had no effect on cell death in RR-#2 cells (Fig. 6A). A flow cytometry analysis revealed that transfection of siPAI-2, siNOMO2, siKLC4, or siPLOD3 alone increased cell death by approximately 20%, 16%, 19%, and

20%, respectively, in RR-#2 cells compared to 7% in untransfected RR-#2 cells (Fig. 6B). Stimulation of the corresponding knockdown cells with 10-Gy radiation synergistically enhanced cell death, increasing it to approximately 34%, 26%, 29%, and 32% in RR-#2 cells compared to 12% in untransfected RR-#2 cells (Fig. 6B). Further support for the cell death effect of target protein knockdown was provided by an examination of the level of the apoptotic marker, cleaved-PARP, which showed that each siRNA substantially up-regulated the level of cleaved-PARP. Notably, the effects of siPAI-2, siNOMO2, siKLC4, and siPLOD3 on cleaved-PARP levels in
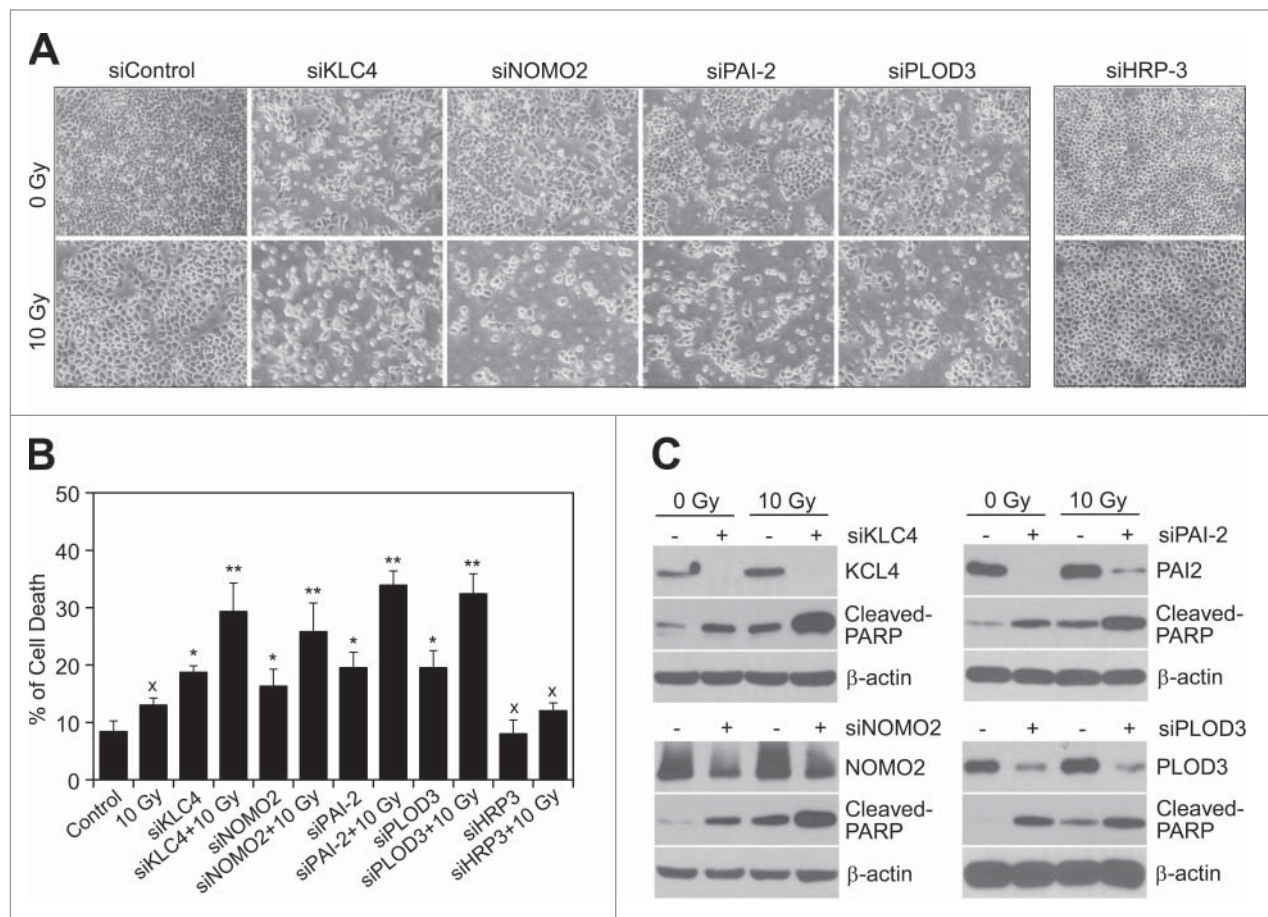
Figure 6. Induction of RR-#2 cell death by individual depletion of 4 novel radioresistance regulatory genes. RR-#2 cells were transfected with 50 nM siKLC4, siNOMO2, siPAI-2, siPLOD3, or control (scrambled) siRNA. siHRP-3 was used as a negative control. After culturing for 24 h, cells were left untreated or were treated with 10-Gy radiation, then incubated for an additional 48 h. (A) Cell morphology was observed by light microscopy. (B) Cell viability was determined by FACS analysis; data are expressed as means ± SD (*$p < 0.05$ and **$p < 0.005$ compared with control; x, not significant). (C) Levels of KCL4, NOMO2, PAI-2, PLOD3, and cleaved-PARP proteins were determined by Western blotting using β-actin as the loading control. The data represent typical results or mean values with standard deviations (n = 4).

RR-#2 cells were additively increased by radiation (Fig. 6C). Collectively, our data suggest that elevated levels of PAI-2, NOMO2, KLC4, and PLOD3 are associated with acquisition of the radioresistance phenotype; thus, these proteins have the capacity to protect H460 cells against radiation-induced apoptosis.

Discussion

Although radiotherapy has made significant contributions to NSCLC treatment, intrinsic or acquired radioresistance of lung tumors remains a critical barrier to attaining the maximal efficacy of radiotherapy. Currently, targeted therapies that interfere with specific cancer genes, proteins, or the tissue environment have been approved for promoting cancer cell death. However, new targeted therapies using novel biomarkers are urgently needed to overcome the radioresistance problem in lung cancer treatment.

In this work, we established RR-H460 cell lines from human radiosensitive parental H460 NSCLC cells by repeated exposure to radiation for use in identifying radioresistance regulatory molecules. Hsp90 and Her-3 proteins have previously been established as determinants of radiosensitivity in a variety of human tumors of different histological origins, including glioma, prostate, cervical, breast and pancreatic cancer.[15,16] Therefore, the Hsp90- and Her-3–upregulated phenotype of RR-H460 cell lines establishes these cells as appropriate cellular models (Fig. 1). Notably, RR-H460 cell lines exhibited CSC characteristics, displaying several aberrant CSC markers, such as CD44, activated Notch1, Nanog, Sox-2, and β-catenin (Fig. 2). From a signal transduction perspective, the CSC-related Wnt/β-catenin, Hedgehog, Notch, JAK/STAT, BMP (bone morphogenic protein), and Akt pathways, or their dysregulation, play a fundamental role in enabling CSCs to retain their unique properties. For example, overexpression of β-catenin promotes CSC properties and tumorigenesis both in vitro and in vivo, suggesting an important role for the Wnt/β-catenin pathway in the regulation of CSC self-renewal.[21] Because components of the Notch signaling network are expressed in lung CSC populations and their expression is frequently deregulated in human malignancies, previous report has suggested that Notch signaling plays a pivotal role in maintaining CSC populations.[22] Recent emerging evidence has indicated that CSCs are more resistant to radiation and anticancer drug therapy than non-CSCs.[21] This property of CSCs is thought to be responsible for cancer metastasis and recurrence despite radiotherapy or chemotherapy, consistent with our demonstration of a malignant phenotype in RR-H460 CSC lines (Figs. 3 and 4). Therefore, innovative radiotherapy approaches targeting radioresistant CSCs might be a key to completely eradicating lung tumors and promoting better outcomes for patients undergoing radiotherapy.

Analyses of expression profiles between radiation responders and non-responders can be useful in predicting the response to radiotherapy. Thus, molecular parameters can provide insights into the development of individualized therapies. Radioresponse-associated gene expression profiles developed based on microarray analyses have been reported in several cancers, including lung, head and neck, and colorectal cancers.

These reports have identified genes associated with DNA repair, apoptosis, cell cycle, metastasis, and hypoxia.[23] Moreover, because protein biomarkers are indicators of physiological states during the disease process, large-scale protein expression arrays are becoming increasingly popular screening strategies.[24] Since Ramsamooj et al. first compared the patterns of protein expression in radiation-resistant and sensitive head-and-neck cancer cells,[25] proteome profiles have been performed in various other cancers, including prostate, breast, rectal, and laryngeal cancers.[14,26] We previously identified aldehyde reductase and INPP4B (inositol polyphosphate-4-phosphatase, type II) as laryngeal cancer radioresistance biomarkers and showed that their signaling is involved in the mechanism underlying resistance to radiation.[27,28] With the exception of 2D electrophoresis assays performed on cisplatin-resistant A549 cells to evaluate whether multidrug resistance contributes to elevated radioresistance,[18] no proteomic approaches for predicting radioresistance biomarkers have been reported in lung cancer. Here, using a comparative proteomic analysis employing 2D electrophoresis and MALDI-TOF mass spectrometry analyses, we identified 8 proteins that showed significantly increased expression in RR-H460 CSC lines compared with H460 cells (Table 1). Based on their functions, 3 of these proteins—FASN, VIM and GRP78—had previously been identified as prognostic markers of radiotherapy resistance in various tumors, including nasopharyngeal carcinoma, lung cancer, and head-and-neck cancer.[17-19] Our results also showed that the expression of these 3 proteins was much higher in RR-H460 CSC lines than in parental H460 cells (Fig. 5B). Interestingly, the previously identified radioresponse-associated protein UQCRC1, which was shown to be decreased by radiation or arsenite treatment in human TK6 lymphoblastoid cells,[20] was found to be increased in RR-H460 CSC lines established by repeated irradiation of H460 cells. This difference may reflect differences in cell line and treatment methods. In addition to adding these 4 known proteins to the list of radioresistance and/or CSC biomarkers in NSCLC cells, we identified PAI-2, NOMO2, KLC4, and PLOD3 as potential biomarkers. PAI-2 is a secreted protein that inhibits tumor necrosis factor (TNF)-α–mediated apoptosis in HeLa cells, indicating that PAI-2 might be an important factor in regulating cell death in TNF-mediated inflammatory processes.[29] Members of the NOMO family are associated with cancer progression, stem cell maintenance, and differentiation,[30] but the cellular functions of NOMO2 are currently largely unknown. KLC4 contributes to fundamental cellular functions such as survival and morphogenesis by interacting with members of the kinesin superfamily to regulate microtubule motor activity and organelle transport.[31] However, functions of KLC4 have not hitherto been linked to cancer. PLOD3 catalyzes the hydroxylation of lysyl residues in collagen-like peptides and was recently identified as a tumorigenesis biomarker in colorectal cancer.[32] However, relatively little is known about the functions of these 4 proteins in the context of radioresistance or the maintenance of CSC-like properties (Table 2). In the current study, we first inferred a radioresistance-inducing role of these proteins from siRNA transfection experiments, which showed that knockdown of each of these individual proteins significantly promoted cell death in RR-H460 CSCs (Fig. 6). Since a tumor-secreted protein could be a

biomarker, the known secreted proteins PAI-2 and PLOD3 might be useful novel diagnostic and prognostic markers of radioresistance in NSCLC cells. The development of diagnostic or prognostic bio-kits will require additional experiments to determine whether NOMO2 and KLC4 are also secreted protein. Notably, we suggest that the 4 newly identified proteins could be used as predictive biomarkers and/or potential therapeutic targets in lung cancer. Although the mechanisms by which target biomarkers determine how a cell becomes more or less sensitive to radiation-induced cell death are poorly understood, we speculate that the radioresistance mechanisms in cancer are regulated through interactions among multiple proteins rather than being caused by a single molecule. Therefore, further information about the 4 novel proteins, such as their involvement in a radioresistance signaling pathway or network, may help develop these biomarkers as a tool to predict the outcome of radiotherapy.

Materials and methods

Cell culture and treatment

Human H460, A549, and H1299 NSCLC cells were purchased from American Type Culture Collection (Manassas, VA). Cells were grown in Roswell Park Memorial Institute medium 1640 (Gibco-BRL, Rockville, MD) containing 10% fetal bovine serum, 50 μg/mL streptomycin, and 50 units/mL penicillin. Cells were irradiated using a [137]cesium-ray source (Atomic Energy of Canada Ltd., Mississauga, Canada) at a dose rate of 3.81 Gy/min.

Establishment of RR-H460 cell lines

The irradiated cell population (RR-Full) with a radioresistant phenotype was established from H460 cells as described previously.[14] Subclones (RR-#2 and RR-#5) isolated from the RR-Full population were selected as RR-H460 variants on the basis of clonogenic survival assays performed following exposure to 6-Gy radiation. Parental H460 cells were maintained as control cells.

Clonogenic assay

Cell survival was determined by clonogenic-survival assay as described previously.[14] Briefly, cells were seeded into triplicate 60-mm tissue culture dishes at densities of 1.2, 2.4, 6.0, and 12.0 $\times 10^3$ cells/dish and exposed to 0, 2, 4, and 6 Gy, respectively. Cells were exposed once to different doses of radiation. After 14 d, colonies arising from surviving cells were stained with trypan blue solution and counted using a colony counter (Imaging Products, Chantilly, VA).

Sphere-forming assay for generation of CSCs

H460 and RR-H460 cell lines were cultured under sphere-forming conditions in a stem cell-permissive medium consisting of DMEM-F12 containing 20 ng/mL epidermal growth factor, 20 ng/mL basic fibroblast growth factor, and B27 serum-free supplement (50X; Life Technologies, Inc., Grand Island,

NY). Spheres were collected after 5 d and protein was extracted for Western blotting.

Detection of cell surface markers

Cells were washed with phosphate-buffered saline (PBS) and permeabilized with 0.1% Triton X-100 in PBS for 5 min. After washing with PBS 3 times, cells were incubated with anti-CD133 (Miltenyi Biotec Inc., San Diego, CA) or CD44 (Life Technologies, Inc.,) antibodies for 30 min and then incubated with fluorescein isothiocyanate (FITC)-conjugated secondary antibody for 20 min. After washing with PBS twice, cells were analyzed by fluorescence-activated cell sorting (FACS) on a flow cytometer (Becton Dickson, Franklin Lakes, NJ).

Cell proliferation. Cells were plated on 60-mm dishes at a density of 3×10^5 cells. At each time point, cell proliferation was determined by direct cell counting using a hemocytometer.

Apoptosis analysis. Cells seeded at a density of 7×10^5 cells per 60-mm dish were left untreated or were treated with 10-Gy radiation for 48 h. Cell death was determined and quantified as described previously.[33]

Cell cycle analysis. Cells were pelleted in PBS and fixed in cold 70% ethanol for 2 h at 4°C. Cells were treated with 100 mg/mL ribonuclease for 1 h on ice and subsequently stained with 5 μg/ml propidium iodide (PI) at room temperature for 15 min. DNA content was analyzed by flow cytometry (Becton Dickson). The Modfit cell-cycle program (Verity Software House Inc., Yopsham, ME) was used to determine the fractions of cells in G_1, S, and G_2/M phases of the cell-cycle distribution.

Western blot analysis

Western blotting was performed as described previously.[34] Blots were probed with primary antibodies against CD44, phospho-p53 (Ser15), Sox2 and cleaved-PARP (Asp214) (Cell Signaling Technology, Beverly, MA); p53, p16, KCL4, Oct4 and PAI2 (Santa Cruz Biotechnology Inc., Santa Cruz, CA); Nanog and activated Notch1 (EMD Millipore Corporation, Billerica, MA); NOMO2 and PLOD3 (Proteintech Group, Inc., Chicago, IL); and p21 (BD Bioscience, San Jose, CA). β-Actin (Sigma) was used as a loading control.

Quantitative reverse transcription-polymerase chain reaction

Transcripts were quantified by qRT-PCR as described previously[34] using the following primer pairs: Hsp90, 5′-TTG GAG GAA CGA AGA ATA G-3′ (sense) and 5′-GGG CTC TGA ATT CCA ACT GTC-3′ (antisense), yielding a 427-bp product; Her-3, 5′-TCT GAA TGG CCT GAG TGT G-3′ (sense) and 5′-TGG GTC ATC ATC AAG GAG-3′ (antisense), yielding a 400-bp product; glyceraldehyde-3-phophate dehydrogenase (GAPDH), 5′-CAT CTC TGC CCC CTC TGC TGA-3′ (sense) and 5′-GGA TGA CCT TGC CCA CAG CCT-3′ (antisense), yielding a 305-bp product. A two-temperature thermocycling program was used, with 42 cycles of 95°C (denaturation) and 55°C (annealing). The amplification signal from target genes

was normalized against the cycle threshold values of GAPDH in the same reaction.

Knockdown of genes

The following human specific siRNAs, synthesized as described by the manufacturer (Genolution, Seoul, Korea), were used: siKLC4, 5′-CCA GAA UAA GUA UAA GGA AUU-3′; siNOMO2, 5′-GCA GAU UAA UCA AUU UGA UUU-3′; siPAI-2, 5′-CAC UCU UUG CCC UCA AUU UUU-3′; and siPLOD3, 5′-GGA AGU ACA AGG AUG AUG AUU-3′. Scrambled siRNAs, which showed no significant homology to known gene sequences and did not regulate expression, were used as negative controls. Cells were transiently transfected with 50 nM siRNA in medium supplemented with FBS using Lipofectamine RNAiMAX reagent (Life Technologies, Inc.,), according to the manufacturer's protocol. The depletion of target proteins was confirmed by Western blot analysis.

Wound-healing assay

Cells were grown in 60-mm dishes until forming confluent monolayers. Cell monolayers were scratched with a 200-μL pipette tip, then washed twice with PBS and incubated in fresh medium. Marked wounds were photographed at the indicated time points using an inverted microscope (TE300, Nikon, Japan).

Invasion and migration assays

Invasion assays were done using 1.5×10^5 cells in BD BioCoat Matrigel Invasion Chambers (Becton Dickinson), pre-coated with 10 mg/mL growth factor-reduced Matrigel on the upper side of the chamber, according to the manufacturer's instructions. Migration assays were performed using essentially the same procedures, but without pre-coated chambers. Invaded and migrated cells were fixed and stained with a Diff-Quick kit (Fisher Scientific Inc., Waltham, MA). Cells in 5 randomly selected fields were imaged under a microscope (MZ16FA, Leica, Germany) and counted.

Soft agar colony-formation assay

Cells (1×10^5) were resuspended in 0.4% agarose in culture medium supplemented with 10% FBS and seeded on 0.8% agarose in the same medium in 60-mm dishes. Cells were cultured for 14 d at 37°C in a humidified chamber containing 5% CO_2 and then stained with 0.005% crystal violet. Colonies in 5 randomly selected fields were photographed and evaluated.

SA-β-gal staining

Detection of SA-β-gal activity was performed as described previously.[34] Briefly, cells were fixed with a 3.7% formaldehyde solution for 10 min. After washing twice with PBS, cells were incubated at 37°C with SA-β-gal staining solution consisting of 1 mg/mL of 5-bromo-4-chloro-3-indolyl β-D-galactoside (Promega, Madison, WI), 40 mM citric acid/sodium phosphate buffer (pH 6.0), 5 mM potassium ferrocyanide, 5 mM potassium ferricyanide, 150 mM NaCl, and 2 mM $MgCl_2$. Staining was evaluated after incubating for 16 h in a CO_2-free, 37°C oven

Gel electrophoresis and staining

Parental H460, RR-Full, and RR-#2 cell lines were solubilized in 200 μL of PAGE buffer (9 M urea, 40 mM Tris, 4% CHAPS, pH 8.5), sonicated with a probe sonicator (Branson Ultrasonic Corporation, Danbury), and centrifuged at 12,000 rpm for 15 min. Samples (150 μg) were resolved by isoelectric focusing in the first dimension using IPG strips (pH 4–10) and then resolved in the second dimension by SDS-PAGE on 12% gels. Gels were routinely stained using ammoniacal silver as described previously.[14]

In-gel digestion and mass spectrometry analysis

All silver-stained spots were destained with a 1:1 solution of 30 mM potassium ferricyanide and 100 mM sodium thiosulfate, and then were in-gel digested with 10 ng/mL trypsin (Promega). Dried tryptic peptides were analyzed by mass spectrometry, and proteins were identified by peptide mass fingerprinting as described previously.[14]

Disclosure of potential conflicts of interest

No potential conflicts of interest were disclosed.

Funding

References

1. Anglim PP, Alonzo TA, Laird-Offringa IA. DNA methylation-based biomarkers for early detection of non-small cell lung cancer: an update. Mol Cancer 2008; 7:81-4598-7-81; PMID:18208603; http://dx.doi.org/10.1186/1476-4598-7-81

2. Lazzari C, Spitaleri G, Catania C, Barberis M, Noberasco C, Santarpia M, Delmonte A, Toffalorio F, Conforti F, De Pas TM. Targeting ALK in patients with advanced non small cell lung cancer: biology, diagnostic and therapeutic options. Crit Rev Oncol Hematol 2014; 89: 358-365; PMID:24156959; http://dx.doi.org/10.1016/j.critrevonc.2013.09.003

3. Sirzen F, Kjellen E, Sorenson S, Cavallin-Stahl E. A systematic overview of radiation therapy effects in non-small cell lung cancer. Acta Oncol 2003; 42: 493-515; PMID:14596509; http://dx.doi.org/10.1080/02841860310014453

4. Biard DS, Martin M, Rhun YL, Duthu A, Lefaix JL, May E, May P. Concomitant p53 gene mutation and increased radiosensitivity in rat lung embryo epithelial cells during neoplastic development. Cancer Res 1994; 54: 3361-3364; PMID:8012950

5. Lee JU, Hosotani R, Wada M, Doi R, Kosiba T, Fujimoto K, Miyamoto Y, Tsuji S, Nakajima S, Nishimura Y, Imamura M. Role of bcl-2 family proteins (bax, bcl-2 and bcl-X) on cellular susceptibility to radiation in pancreatic cancer cells. Eur J Cancer 1999; 35: 1374-1380; PMID:10658530; http://dx.doi.org/10.1016/S0959-8049(99)00134-3

6. Ramsamooj P, Kasid U, Dritschilo A. Differential expression of proteins in radioresistant and radiosensitive human squamous carcinoma

cells. J Natl Cancer Inst 1992; 84: 622-628; PMID:1556773; http://dx.doi.org/10.1093/jnci/84.8.622

7. Kim IA, Bae SS, Fernandes A, Wu J, Muschel RJ, McKenna WG, Birnbaum MJ, Bernhard EJ. Selective inhibition of ras, phosphoinositide 3 kinase, and akt isoforms increases the radiosensitivity of human carcinoma cell lines. Cancer Res 2005; 65: 7902-7910; PMID:16140961; http://dx.doi.org/10.1158/0008-5472.CAN-05-0513

8. Vivanco I, Sawyers CL. The phosphatidylinositol 3-kinase AKT pathway in human cancer. Nat Rev Cancer 2002; 2: 489-501; PMID:12094235; http://dx.doi.org/10.1038/nrc839

9. Yun HS, Hong EH, Lee SJ, Baek JH, Lee CW, Yim JH, Um HD, Hwang SG. Depletion of hepatoma-derived growth factor-related protein-3 induces apoptotic sensitization of radioresistant A549 cells via reactive oxygen species-dependent p53 activation. Biochem Biophys Res Commun 2013; 439: 333-339; PMID:24012673; http://dx.doi.org/10.1016/j.bbrc.2013.08.086

10. Yun HS, Baek JH, Yim JH, Lee SJ, Lee CW, Song JY, Um HD, Park JK, Park IC, Hwang SG. Knockdown of hepatoma-derived growth factor-related protein-3 induces apoptosis of H1299 cells via ROS-dependent and p53-independent NF-kappaB activation. Biochem Biophys Res Commun 2014; 449: 471-476; PMID:24857986; http://dx.doi.org/10.1016/j.bbrc.2014.05.039

11. Nojiri K, Iwakawa M, Ichikawa Y, Imadome K, Sakai M, Nakawatari M, Ishikawa K, Ishikawa A, Togo S, Tsujii H, Shimada H, Imai T. The proangiogenic factor ephrin-A1 is up-regulated in radioresistant murine tumor by irradiation. Exp Biol Med (Maywood) 2009; 234: 112-122; PMID:18997097; http://dx.doi.org/10.3181/0806-RM-189

12. Guo WF, Lin RX, Huang J, Zhou Z, Yang J, Guo GZ, Wang SQ. Identification of differentially expressed genes contributing to radioresistance in lung cancer cells using microarray analysis. Radiat Res 2005; 164: 27-35; PMID:15966762; http://dx.doi.org/10.1667/RR3401

13. Lee YS, Oh JH, Yoon S, Kwon MS, Song CW, Kim KH, Cho MJ, Mollah ML, Je YJ, Kim YD, Kim CD, Lee JH. Differential gene expression profiles of radioresistant non-small-cell lung cancer cell lines established by fractionated irradiation: Tumor protein p53-inducible protein 3 confers sensitivity to ionizing radiation. Int J Radiat Oncol Biol Phys 2010; 77: 858-866; PMID:20510196; http://dx.doi.org/10.1016/j.ijrobp.2009.12.076

14. Kim JS, Chang JW, Yun HS, Yang KM, Hong EH, Kim DH, Um HD, Lee KH, Lee SJ, Hwang SG. Chloride intracellular channel 1 identified using proteomic analysis plays an important role in the radiosensitivity of HEp-2 cells via reactive oxygen species production. Proteomics 2010; 10: 2589-2604; PMID:20461716; http://dx.doi.org/10.1002/pmic.200900523

15. Camphausen K, Tofilon PJ. Inhibition of Hsp90: A multitarget approach to radiosensitization. Clin Cancer Res 2007; 13: 4326-4330; PMID:17671112; http://dx.doi.org/10.1158/1078-0432.CCR-07-0632

16. Contessa JN, Abell A, Mikkelsen RB, Valerie K, Schmidt-Ullrich RK. Compensatory ErbB3/c-src signaling enhances carcinoma cell survival to ionizing radiation. Breast Cancer Res Treat 2006; 95: 17-27; PMID:16267617; http://dx.doi.org/10.1007/s10549-005-9023-9

17. Kao YC, Lee SW, Lin LC, Chen LT, Hsing CH, Hsu HP, Huang HY, Shiue YL, Chen TJ, Li CF. Fatty acid synthase overexpression confers an independent prognosticator and associates with radiation resistance in nasopharyngeal carcinoma. Tumour Biol 2013; 34: 759-768; PMID:23208675; http://dx.doi.org/10.1007/s13277-012-0605-y

18. Wei R, Zhang Y, Shen L, Jiang W, Li C, Zhong M, Xie Y, Yang D, He L, Zhou Q. Comparative proteomic and radiobiological analyses in human lung adenocarcinoma cells. Mol Cell Biochem 2012; 359: 151-159; PMID:21822689; http://dx.doi.org/10.1007/s11010-011-1008-x

19. Wu MJ, Jan CI, Tsay YG, Yu YH, Huang CY, Lin SC, Liu CJ, Chen YS, Lo JF, Yu CC. Elimination of head and neck cancer initiating cells through targeting glucose regulated protein78 signaling. Mol Cancer 2010; 9:283-4598-9-283; PMID:20085644; http://dx.doi.org/10.1186/1476-4598-9-283

20. Tapio S, Danescu-Mayer J, Asmuss M, Posch A, Gomolka M, Hornhardt S. Combined effects of gamma radiation and arsenite on the proteome of human TK6 lymphoblastoid cells. Mutat Res 2005; 581: 141-152; PMID:15725613; http://dx.doi.org/10.1016/j.mrgentox.2004.11.016

21. Nguyen GH, Murph MM, Chang JY. Cancer stem cell radioresistance and enrichment: where frontline radiation therapy may fail in lung and esophageal cancers. Cancers (Basel) 2011; 3: 1232-1252; PMID:21603589; http://dx.doi.org/10.3390/cancers3011232

22. Levina V, Marrangoni AM, DeMarco R, Gorelik E, Lokshin AE. Drug-selected human lung cancer stem cells: cytokine network, tumorigenic and metastatic properties. PLoS One 2008; 3: e3077; PMID:18728788; http://dx.doi.org/10.1371/journal.pone.0003077

23. Ogawa K, Murayama S, Mori M. Predicting the tumor response to radiotherapy using microarray analysis (review). Oncol Rep 2007; 18: 1243-1248; PMID:17914580; http://dx.doi.org/10.3892/or.18.5.1243

24. Srinivas PR, Kramer BS, Srivastava S. Trends in biomarker research for cancer detection. Lancet Oncol 2001; 2: 698-704; PMID:11902541; http://dx.doi.org/10.1016/S1470-2045(01)00560-5

25. Ramsamooj P, Kasid U, Dritschilo A. Differential expression of proteins in radioresistant and radiosensitive human squamous carcinoma cells. J Natl Cancer Inst 1992; 84: 622-628; PMID:1556773; http://dx.doi.org/10.1093/jnci/84.8.622

26. Lacombe J, Azria D, Mange A, Solassol J. Proteomic approaches to identify biomarkers predictive of radiotherapy outcomes. Expert Rev Proteomics 2013; 10: 33-42; PMID:23414358; http://dx.doi.org/10.1586/epr.12.68

27. Kim JS, Chang JW, Park JK, Hwang SG. Increased aldehyde reductase expression mediates acquired radioresistance of laryngeal cancer cells via modulating p53. Cancer Biol Ther 2012; 13: 638-646; PMID:22555805; http://dx.doi.org/10.4161/cbt.20081

28. Kim JS, Yun HS, Um HD, Park JK, Lee KH, Kang CM, Lee SJ, Hwang SG. Identification of inositol polyphosphate 4-phosphatase type II as a novel tumor resistance biomarker in human laryngeal cancer HEp-2 cells. Cancer Biol Ther 2012; 13: 1307-1318; PMID:22895072; http://dx.doi.org/10.4161/cbt.21788

29. Dickinson JL, Bates EJ, Ferrante A, Antalis TM. Plasminogen activator inhibitor type 2 inhibits tumor necrosis factor alpha-induced apoptosis: evidence for an alternate biological function. J Biol Chem 1995; 270: 27894-27904; PMID:7499264; http://dx.doi.org/10.1074/jbc.270.46.27894

30. Topczewska JM, Postovit LM, Margaryan NV, Sam A, Hess AR, Wheaton WW, Nickoloff BJ, Topczewski J, Hendrix MJ. Embryonic and tumorigenic pathways converge via nodal signaling: Role in melanoma aggressiveness. Nat Med 2006; 12: 925-932; PMID:16892036; http://dx.doi.org/10.1038/nm1448

31. Hirokawa N, Noda Y, Tanaka Y, Niwa S. Kinesin superfamily motor proteins and intracellular transport. Nat Rev Mol Cell Biol 2009; 10: 682-696; PMID:19773780; http://dx.doi.org/10.1038/nrm2774

32. Nicastri A, Gaspari M, Sacco R, Elia L, Gabriele C, Romano R, Rizzuto A, Cuda G. N-glycoprotein analysis discovers new up-regulated glycoproteins in colorectal cancer tissue. J Proteome Res 2014; 13: 4932-4941; PMID:25247386; http://dx.doi.org/10.1021/pr500647y

33. Kim MJ, Yun HS, Hong EH, Lee SJ, Baek JH, Lee CW, Yim JH, Kim JS, Park JK, Um HD, Hwang SG. Depletion of end-binding protein 1 (EB1) promotes apoptosis of human non-small-cell lung cancer cells via reactive oxygen species and bax-mediated mitochondrial dysfunction. Cancer Lett 2013; 339: 15-24; PMID:23900080; http://dx.doi.org/10.1016/j.canlet.2013.07.027

34. Hong EH, Lee SJ, Kim JS, Lee KH, Um HD, Kim JH, Kim SJ, Kim JI, Hwang SG. Ionizing radiation induces cellular senescence of articular chondrocytes via negative regulation of SIRT1 by p38 kinase. J Biol Chem 2010; 285: 1283-1295; PMID:19887452; http://dx.doi.org/10.1074/jbc.M109.058628